

Analysis of Multiplication Characteristics of Coaxial Waveguide Loaded Ceramic under External Electric Field

Long Yao^{1, 2}, Rui Zhang^{1, *}, Yong Wang¹, and Xue Zhang³

Abstract—Multipacting is electron discharge that occurs in components operating in RF high-power electromagnetic fields. In this paper, we will study a new coaxial structure with a ceramic window. A similar structure is utilized in many high power devices for power transfer. Due to the multipactor effect, it will generate huge heat and cause damage to the window, ultimately affect the performance of microwave devices. In order to suppress the surface multipactor effect and improve the transmitting power, the application of an external DC bias is analyzed and simulated. A Monte Carlo algorithm is used to track the secondary electron trajectories and study the multipactor scenario on the surface of a ceramic window in a coaxial line by using 2-D particles distribution code. Since secondary electron multiplication needs to meet specific resonance conditions, an appropriate DC bias will generate a compensating trajectory and collision, which can suppress the secondary electron avalanche. The optimal value of this external bias voltage that will avoid the multipactor phenomenon in the coaxial line will be calculated by simulation in MATLAB.

1. INTRODUCTION

The multipactor effect is a resonant vacuum electron discharge that appears in vacuum devices operating in RF high-power electromagnetic field [1]. This phenomenon is present in many different situations, such as RF satellite payload [2–4], particle accelerators, klystrons, and cyclotrons [5]. When specific conditions are satisfied, the free electrons synchronize with the RF electric field and impact against the metallic walls or the ceramic walls releasing secondary electrons. Thus, the increase of the electron population on the device leads to an electrical discharge that leads to remarkable power losses and heating of the wall, so it becomes impossible to increase the fields by raising the incident power [6]. Especially, in the superconducting structures, it is necessary to maintain a low heat state, and the huge heat can lead to a thermal breakdown. Furthermore, a heavy bombing of multipacting electrons may break the ceramic windows leading to disastrous consequences, which will affect the stability of the high power microwave devices.

A general cure against multipacting is to avoid the resonant conditions by either a proper choice of the geometry or by coating the critical area with a material with a lower secondary yield [7, 8]. However, in many circumstances, we cannot make a big difference to the geometry of the device and coating, which are often used to suppress the multiplication, but it cannot completely suppress multipactor, leading to that the success rate of the reduced secondary yield is often failed. In those cases, other suppressing methods must be applied, like static electric or magnetic perturbations, or grooving the surfaces, etc. In this paper, an external DC bias is used on a particular system, a coaxial line loaded ceramic window, to avoid the local resonant multipactor [9, 10]. Moreover, in order to simulate the

Received 15 July 2019, Accepted 19 September 2019, Scheduled 9 October 2019

* Corresponding author: Rui Zhang (ylong0220@sina.com).

¹ Key Laboratory of Science and Technology on High Power Microwave Sources and Technologies, Institute of Electronics, Chinese Academy of Sciences, Beijing 100190, China. ² University of Chinese Academy of Sciences, Beijing 100190, China. ³ Xiangtan University, Xiangtan 411100, China.

actual motion of the free electron in detail, we consider the Coulomb repulsive force and the elastic loss of electron collision. Coulomb repulsion among electrons is modeled by means of a single electron sheet, following the same procedure proposed in [11, 15]. We define an attenuation factor F_{loss} to represent the loss of electron collision in the MATLAB code. In Section 2, we introduce the theory of secondary electron multiplication and make some changes for collisions when the impacting electron is in low energy state. Next, a Monte Carlo (MC) simulation model of the multipactor is introduced, which includes a 2-D particles distribution program. Then we demonstrate the multipactor on the surface of a hollow cylindrical ceramic window in Section 3. The feasibility of using an external DC bias to suppress secondary electron multiplication is discussed in Section 4. Finally, some conclusions are presented in Section 5.

2. MONTE CARLO SIMULATION MODEL

A schematic of a simple hollow cylindrical ceramic window is shown in Fig. 1. The ceramic window and coaxial waveguide are always concentric.

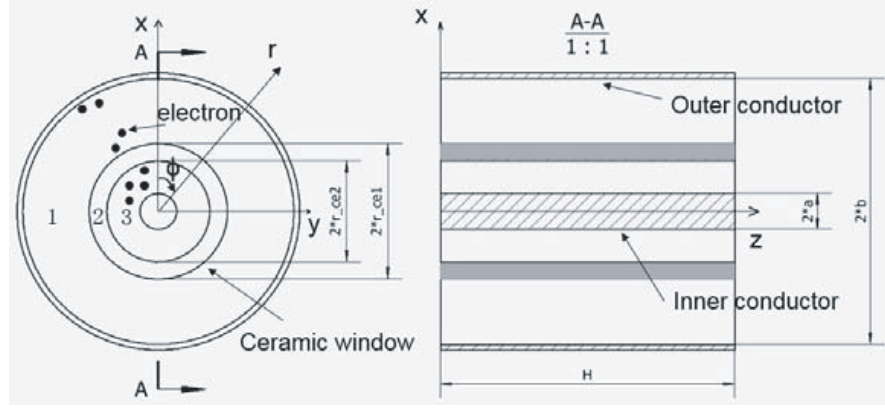


Figure 1. Hollow cylindrical ceramic window in the coaxial line.

The structure considered is a coaxial line with an outer conductor radius $b = 46$ mm and an inner conductor radius $a = 6.25$ mm. The length of the coaxial line is $H = 100$ mm. The hollow cylindrical ceramic window has an outer radius $r_{ce1} = 23.5$ mm and an inner radius $r_{ce2} = 17.5$ mm. The structure is divided into three regions. Region 1 is between the outer conductor and the ceramic, filled with a vacuum at $r_{ce1} < r < b$; region 2 is the dielectric region at $r_{ce2} < r < r_{ce1}$; region 3 is between the ceramic and inner conductor, also filled with a vacuum at $a < r < r_{ce2}$. This article only considers the main mode of the coaxial line TEM mode. Thus, the amplitude of the electric field will be inversely proportional to the distance from the center of the line. Considering the symmetry of the structure, there will be no dependence on the angle around the coaxial axis, which means that the circumstance can be studied as a two-dimensional problem. Denote f as the frequency, and the electric field can be written as:

$$\mathbf{E}_1 = \frac{U_0}{x \left[\ln \left(\frac{b r_{ce2}}{a r_{ce1}} \right) + \frac{1}{\epsilon_r} \ln \left(\frac{r_{ce1}}{r_{ce2}} \right) \right]} e^{-j\beta z} \mathbf{e}_x, \quad r_{ce1} < x < b \quad (1)$$

$$\mathbf{E}_2 = \frac{U_0}{x \epsilon_r \left[\ln \left(\frac{b r_{ce2}}{a r_{ce1}} \right) + \frac{1}{\epsilon_r} \ln \left(\frac{r_{ce1}}{r_{ce2}} \right) \right]} e^{-j\beta z} \mathbf{e}_x, \quad r_{ce2} < x < r_{ce1} \quad (2)$$

$$\mathbf{E}_3 = \frac{U_0}{x \left[\ln \left(\frac{b r_{ce2}}{a r_{ce1}} \right) + \frac{1}{\epsilon_r} \ln \left(\frac{r_{ce1}}{r_{ce2}} \right) \right]} e^{-j\beta z} \mathbf{e}_x, \quad a < x < r_{ce2} \quad (3)$$

$$P = \sum_{i=1}^3 \pi \frac{U_i^2}{\eta_i \ln \left(\frac{R_i}{R_{i-1}} \right)} \quad (4)$$

Here, \mathbf{E}_i ($i = 1, 2, 3$) is the strength of the electric field and magnetic field $\mathbf{H}_i = \frac{1}{\eta_i} \mathbf{z} \times \mathbf{E}_i$; $U_0 = \sum_{i=1}^3 U_i$ is the voltage of the inner and outer conductor; P is the transmission power in the coaxial line; $\beta = w\sqrt{\mu_0 \varepsilon_{eff} \varepsilon_0}$ and $\varepsilon_{eff} = \frac{\ln(b/a)}{\ln(b*r_{ce2}/a/r_{ce1}) + \ln(r_{ce1}/r_{ce2})/\varepsilon_r}$ are the propagation constant in the z -direction and equivalent permittivity in coaxial line loaded ceramic [12], respectively; $\eta_i = \sqrt{\mu_0/(\varepsilon_{ri}\varepsilon_0)}$ is the wave impedance; $\varepsilon_r = 9.4$ is the relative permittivity of ceramic; \mathbf{e}_x is the direction of radial in the cylindrical coordinate system.

In this paper, we use a Monte Carlo code to perform the simulations of multipactor in the coaxial lines using the traditional single effective electron model [13, 14]. The initial particles (N_e) are randomly distributed in the computation space and consequently driven by an electromagnetic force. Consider the Coulomb repulsion among free electrons by means of a single electron sheet. This electronic sheet structure is cylindrically shaped. Considering that the entire structure is divided into two parts, we assume that there are two electronic clouds. One of them is between the outer conductor and the ceramic window, and the other is between the ceramic window and inner conductor. Correspondingly, the radius of the electronic sheet is $r_{s1} = (b + r_{ce1})/2$ and $r_{s2} = (r_{ce2} + a)/2$ the center of the coaxial gap. The related electrical density charge is given by the following: $\rho_{s1} = -\frac{eN_1(t)}{2\pi r_{s1}H}$ and $\rho_{s2} = -\frac{eN_3(t)}{2\pi r_{s2}H}$, where N_1 and N_3 are the number of electrons at regions 1 and 3, respectively. Therefore, using Gauss's law the spacecharge field can be expressed as follows [15]:

$$\mathbf{E}_{sc1} = \begin{cases} -\frac{r_{s1} \rho_{s1}}{x \varepsilon_0} \frac{\ln\left(\frac{b}{r_{s1}}\right)}{\ln\left(\frac{r_{ce1}}{b}\right)} \mathbf{e}_x & r_{ce1} < x \leq r_{s1} \\ \frac{r_{s1} \rho_{s1}}{x \varepsilon_0} \frac{\ln\left(\frac{r_{s1}}{r_{ce1}}\right)}{\ln\left(\frac{b}{r_{ce1}}\right)} \mathbf{e}_x & r_{s1} < x \leq b \end{cases} \quad \mathbf{E}_{sc2} = \begin{cases} -\frac{r_{s2} \rho_{s2}}{x \varepsilon_0} \frac{\ln\left(\frac{r_{ce2}}{r_{s2}}\right)}{\ln\left(\frac{r_{ce2}}{a}\right)} \mathbf{e}_x & a < x \leq r_{s2} \\ \frac{r_{s2} \rho_{s2}}{x \varepsilon_0} \frac{\ln\left(\frac{r_{s2}}{a}\right)}{\ln\left(\frac{r_{ce2}}{a}\right)} \mathbf{e}_x & r_{s2} < x \leq r_{ce2} \end{cases} \quad (5)$$

The assumption that the positive charge on the hollow cylindrical ceramic window is uniformly distributed on the surface. This assumption leads to the simple form of Equation (7) by Gauss' law. Then it is assumed that electron dynamics is governed by the Newton-Lorenz equation (6) using the Runge-Kutta method to compute electron trajectory.

$$\frac{\partial^2 \mathbf{l}}{\partial t^2} = \frac{-e}{m} \left(\mathbf{E}_i + \mathbf{E}_{sc1} + \mathbf{E}_{sc2} + \mathbf{E}_{dc} + \frac{\partial \mathbf{l}}{\partial t} \times \mathbf{B}_i \right) \quad (6)$$

$$\mathbf{E}_{dc} = \frac{eN}{2\pi\varepsilon_0 x H} \mathbf{e}_x \quad (7)$$

Here, \mathbf{l} is the trajectory of the electron; \mathbf{E}_i and $\mathbf{B}_i = \mu_0 \mathbf{H}_i$ ($i = 1, 3$) denote the RF electric and magnetic fields, respectively; \mathbf{E}_{dc} is the electrostatic field by accumulative charge along x -axis direction; e and m are the charge and mass of an electron; N is the number of cumulative charge of the ceramic window. Due to the axial symmetry of the structure, we only consider the radial and axial components. Thereby, the electron dynamics is governed by the non-relativistic Newton-Lorenz equation (8) and (9)

$$\frac{dv_x}{dt} = \frac{d^2 x}{dt^2} - x \left(\frac{d\phi}{dt} \right)^2 = -\frac{e}{m} [E_i(\mathbf{x}, t) + E_{sc1}(\mathbf{x}, t) + E_{sc2}(\mathbf{x}, t) + E_{dc}(\mathbf{x}, t) - B_i(\mathbf{x}, t)v_z] \quad (8)$$

$$\frac{dv_z}{dt} = \frac{d^2 z}{dt^2} = -\frac{e}{m} [B_i(\mathbf{x}, t)v_x] \quad (9)$$

Here, v_x and v_z are the corresponding components of the electron velocity.

Each effective electron evolves in time by colliding with the coaxial metallic wall or the ceramic wall in the coaxial line. Once the free electrons have impact on the boundary, the secondary electron yield (SEY) function (δ) is computed as a function of the impact kinetic energy and impinging angle by means of the SEY model formulated [16]. We use Vaughan's model equation (10) to compute the SEY. For each secondary electron emitted from the surface of the ceramic and metallic walls, we assume that it has a random emission energy (W_0), which is determined by the Maxwell-Boltzmann distribution with $f(W_0) = \frac{W_0}{W_{0m}^2} e^{-W_0/W_{0m}}$, where $W_{0m} = 0.005 * W_{\max 0}$ is the peak of the distribution of emission energy and given in eV. Emission angle (ϕ) is determined by the following distribution function $g(\phi) = \frac{1}{2} \sin(\phi)$, $0 < \phi < \pi$, which obeys a sinusoidal distribution function [17, 18].

For given values of \mathbf{E}_i , \mathbf{E}_{dc} , \mathbf{E}_{sc1} , \mathbf{E}_{sc2} , and \mathbf{B}_i , the equation of motion is solved numerically to compute the trajectory of the emitted electrons. These emitted electrons will have impact again at the ceramic window surface or the metallic wall to produce more secondary electrons under the action of electric and magnetic fields. At each impact, the impact energy (W_i) and angle (ξ_i) are calculated by $W_i = \frac{1}{2} m(v_x^2 + v_z^2)$ and $\xi = \arctan(\frac{v_z}{v_x})$, respectively. Using W_i and ξ , the secondary electron yield δ is calculated based on Vaughan's model. The simulation process is shown in Fig. 2.

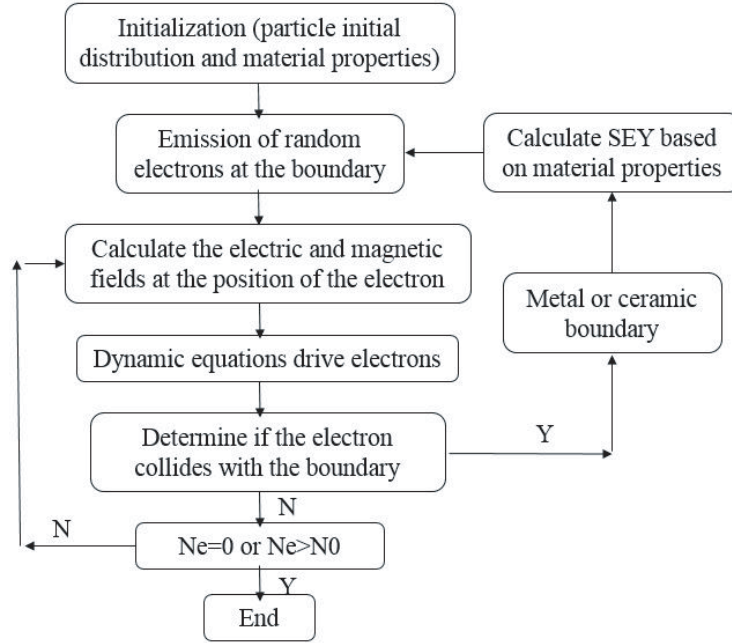


Figure 2. Flowchart of the full design.

In this paper, the parameters of Vaughan's empirical formula are modified to fit experimental results of secondary electron emission yields from an alumina window coated with TiN film that was obtained at the Japanese National Laboratory for High Energy Physics (KEK) [18, 19]. When the impact electrons are at a low energy state ($< W_{th} = 12.5$ eV), the calculation result of secondary electron yield is approximately 0 in this model. It does not match the actual physical process. In the physical process of actual electron collision motion, there is a 30% probability that elastic emission will occur and 70% probability that electron will have energy loss for the impact electrons [20]. Therefore, we define an attenuation factor F_{loss} ($0.2 < F_{loss} < 1$) to represent the energy loss of electron collision in the MATLAB code. This model proposes the following expressions for the total SEY curve.

$$\delta(W, \xi) = \begin{cases} \delta_{low} & \text{for } \gamma < 0 \\ \delta_{\max}(\xi)(\gamma e^{1-\gamma})^k & \text{for } k = \begin{cases} 0.56 & 0 \leq \gamma < 1 \\ 0.903 & 1 \leq \gamma \leq 2 \end{cases} \\ \delta_{\max}(\xi) \frac{1.125}{\gamma^{0.57}} & \text{for } \gamma > 2 \end{cases} \quad (10)$$

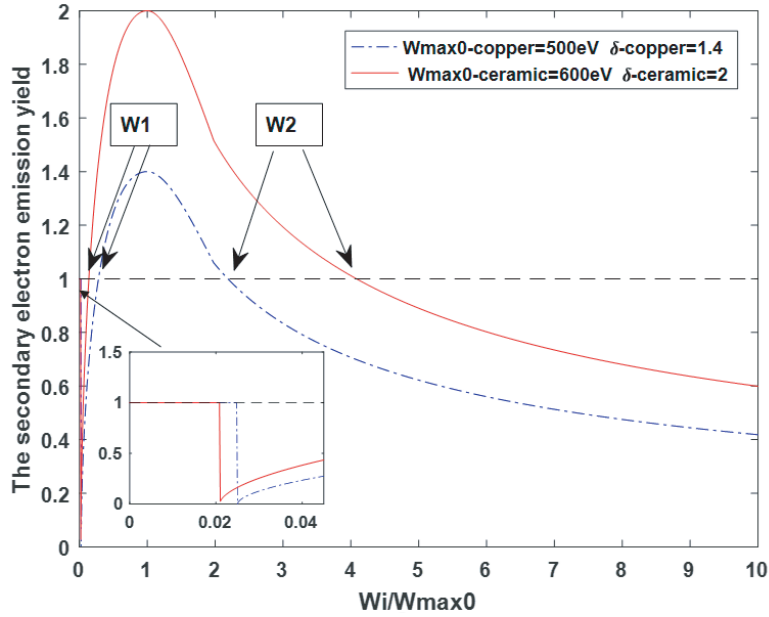


Figure 3. Dependence of secondary electron yield δ on normalized impact energy $W_i/W_{\max 0}$ for different $\delta_{\max 0}$.

where $\gamma = \frac{W_i - W_{th}}{W_{\max}(\xi) - W_{th}}$, $\delta_{\max}(\xi) = \delta_{\max 0}(1 + \frac{k_s \xi^2}{2\pi})$, $W_{\max}(\xi) = W_{\max 0}(1 + \frac{k_s \xi^2}{2\pi})$, and $\delta_{\max 0}$ is the maximum SEY value at normal incidence; $W_{\max 0}$ is the impact kinetic energy at $\delta_{\max 0}$; W_{th} is a parameter obtained from continuity conditions of the SEY curve and physically related to the work function of the material, in which general value is $W_{th} = 12.5$ eV; δ_{low} is the SEY at low impacting energy (within the range from 0 to 1, here, taken equal to 1), which impact electrons produce elastic collision; k_s is a factor related to the surface roughness (here, taken equal to 1).

The secondary electron yield δ at $\xi = 0$ as a function of the normalized impact energy $W_i/W_{\max 0}$ is shown in Fig. 3 for alumina (Al_2O_3) and copper. The first and second crossed-over points are also plotted in Fig. 3. Obviously, these two parameters ($W1$ and $W2$) determine two energies for which the yield is unity. The secondary electron multiplication phenomenon occurs when the incident particle energy is between $W1$ and $W2$, where $\delta > 1$. Meanwhile, the major difference between the secondary yield curve for the copper and alumina (Al_2O_3) is that the copper has a lower maximum yield and lower multiplication interval. Table 1 shows the secondary electron emission (SEE) yields parameters for copper and ceramic.

Table 1. The relevant SEE material properties.

Parameters	Copper	Ceramic
$\delta_{\max 0}$	1.4	2
$W_{\max 0}$	500 eV	600 eV
The first cross-over point	140.4 eV	83.28 eV
The second cross-over point	1093.5 eV	2448 eV

3. MULTIFACTOR CHARACTERISTIC IN A NON-UNIFORM FIELD

Secondary electron multiplication can be roughly divided into tangent multiplication and normal multiplication. In tangent multiplication, free electrons obtain energy from the tangential electric field. In normal multiplication, free electrons gain energy from the normal electric field. The secondary

electron multiplication on the surface of the hollow cylindrical window can be regarded as the standard normal multiplication. In the early stage of multiplication, the electron's transit time is very long, and the electrons moving under the non-uniform field are subject to the ponderomotive force \mathbf{F}_p [21–23], which causes the electron to be subjected to a force pointing to the positive x -axis. The direction of the ponderomotive force is independent of the positive or negative charge, which always points to the direction of weakening electric field strength. According to Equations (1) and (3), we can obtain the ponderomotive force analytical expression

$$\mathbf{F}_p = -\frac{e^2}{4m\omega^2} \nabla |E_i|^2 = \frac{e^2}{2m\omega^2} \frac{U_0^2}{\ln^2(b/a)} \frac{1}{x^3} \mathbf{e}_x \quad (11)$$

We assume that the position of the initial electrons is distributed throughout the computation space with a random initial phase, and the particle motion is advanced by the Runge-Kutta method using 2-D particles distribution model. Meanwhile, we record the position of each particle at each moment and plot the particles distribution map. From Fig. 4 to Fig. 6, obviously, when the power is greater than a certain threshold, the total number of electrons increases exponentially with time, which excites

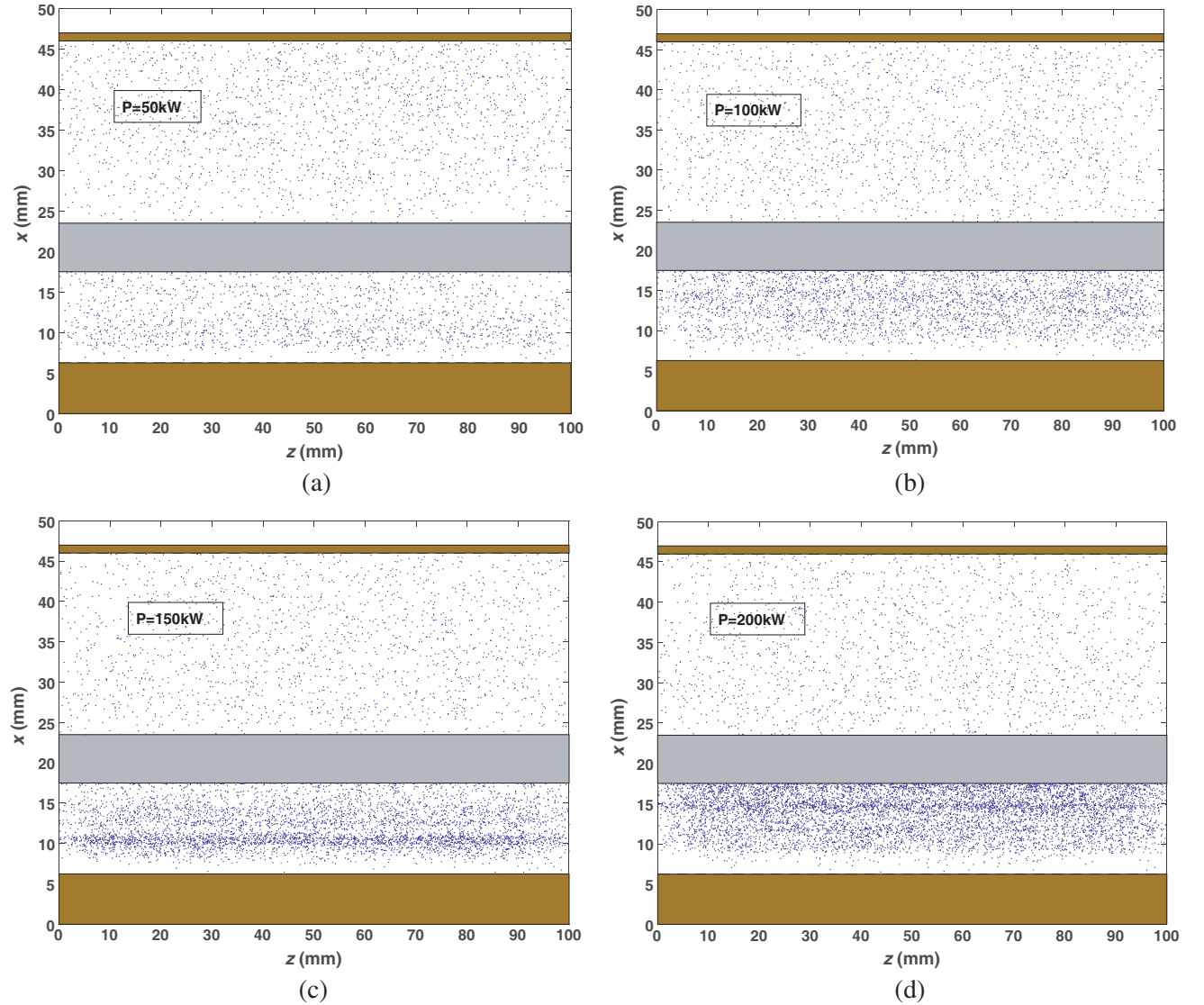


Figure 4. Evolution of the multipactor effect in coaxial line at different powers. $N_e = 6000$, transit time $t = 20$ T, frequency $f = 1.3$ GHz.

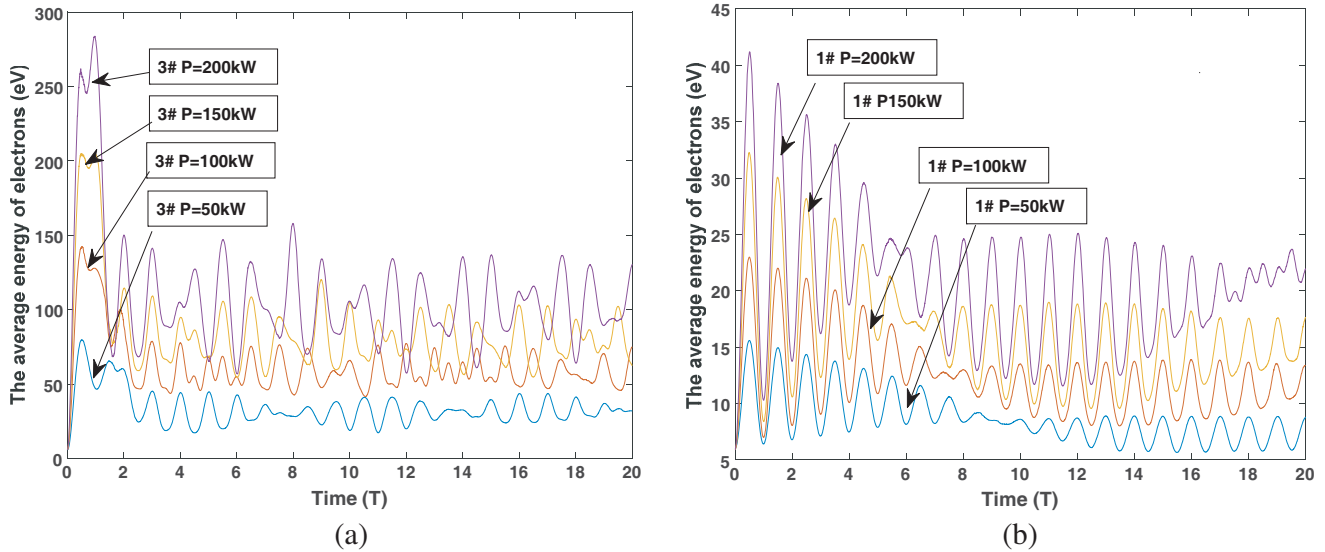


Figure 5. Evolution of the average energy of electrons at different powers. $N_e = 6000$, transit time $t = 20$ T, frequency $f = 1.3$ GHz.

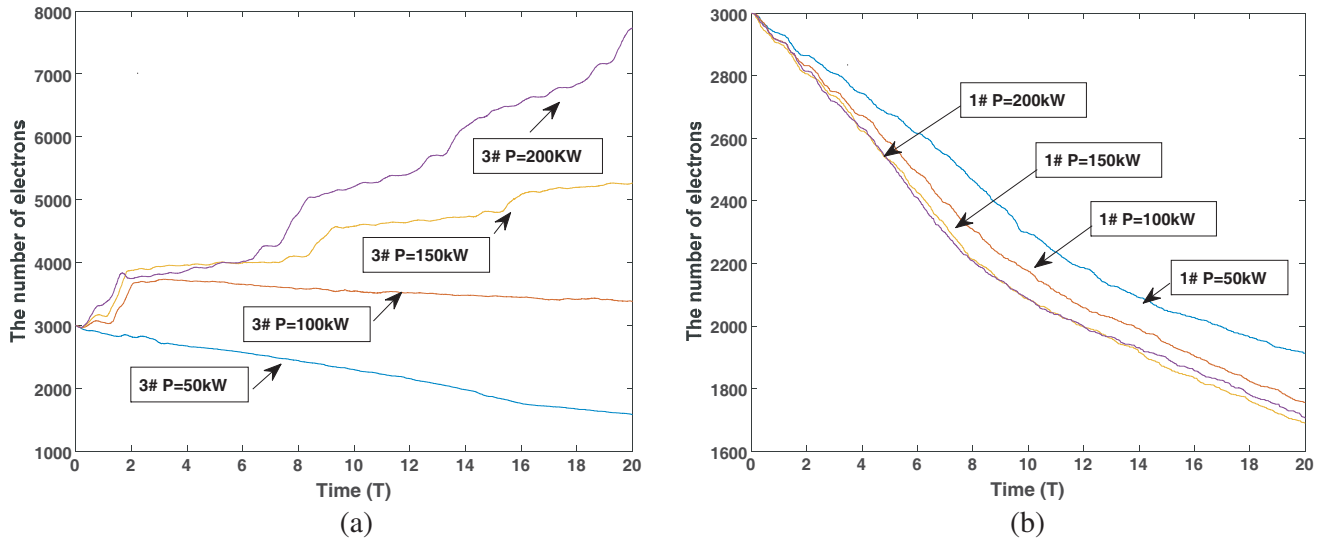


Figure 6. Evolution of the number of electrons at different powers. $N_e = 6000$, transit time $t = 20$ T, frequency $f = 1.3$ GHz.

the secondary electron multiplication phenomenon. In addition, due to the ponderomotive force, the electrons of region 3 area have a convergence of ceramic window boundary. However, this phenomenon does not appear in region 1 area. On the one hand, due to the phenomenon of multipactor, the ceramic window accumulates more and more positive charges, generating a large enough electrostatic field to pull the electrons back to the ceramic surface. On the other hand, the size of the ponderomotive force and electric field is too small to provide enough energy for electronics, which cannot excite the secondary electrons. At the same time, note that the accumulative electric field has no effect on the region 3 area, due to symmetry.

An MC simulation model of a coaxial line in the L-band ($f = 1.3$ GHz) is built using MATLAB code. During calculations, the electrons which pass through the left or right ports will be automatically removed. The multipactor developing stages under different transmission powers are shown in Fig. 4,

including $P = 50$ kW, 100 kW, 150 kW, and 200 kW. The multipactor phenomenon cannot be excited when $P = 50$ kW because the normal field contributes insufficient energy to the electrons. From Figs. 5(a) and (b), note that the average electron energies are 32.34 eV in region 3 and 7.36 eV in region 1 when $P = 50$ kW, which are outside multipactor region. So the number of electrons decreases with time, shown in Figs. 6(a) and (b). The normal field multipactor occurs when the transmission power increases to $P = 200$ kW. According to Figs. 5(a) and (b), the average electrons energies are 107 eV in region 3 area and 19.07 eV in region 1 area. Because the average impact energy in region 3 is in the multiplication range, the number of electrons is increased exponentially, as shown in Fig. 6(a). However, the average energy in region 1 is 19.07 eV, which is far below the first crossover energy of the inner conductor. Thus, the multipactor growth decreases gradually, as shown in Fig. 6(b).

4. EFFECT OF THE EXTERNAL DC BIAS ON THE MULTIPACTOR

We analyze multipacting (without the DC bias) in the coaxial line loaded ceramic window. Note that there is multipactor phenomenon in region 3 when the transmission power $P = 200$ kW. Therefore, we should consider an effective method to avoid multipacting. A static electric perturbation, i.e., a biasing DC bias voltage, is an attractive choice in the coaxial structure. When the external DC bias is applied to suppress secondary electrons, the Newton-Lorentz equation will be modified to Eq. (12), where \mathbf{E}_{bias} denotes the external electric field.

$$\frac{\partial^2 \mathbf{l}}{\partial t^2} = \frac{-e}{m} \left(\mathbf{E}_i + \mathbf{E}_{dc} + \mathbf{E}_{sc1} + \mathbf{E}_{sc2} + \mathbf{E}_{bias} + \frac{\partial \mathbf{l}}{\partial t} \times \mathbf{B}_i \right) \quad (12)$$

The electron dynamics is governed by the non-relativistic Newton-Lorentz equation (13) and (14).

$$\frac{dv_x}{dt} = \frac{d^2 x}{dt^2} - x \left(\frac{d\phi}{dt} \right)^2 = -\frac{e}{m} [E_i(\mathbf{x}, t) + E_{dc}(\mathbf{x}, t) + E_{sc1}(\mathbf{x}, t) + E_{sc2}(\mathbf{x}, t) + E_{bias}(\mathbf{x}, t) - B_i(\mathbf{x}, t)v_z] \quad (13)$$

$$\frac{dv_z}{dt} = \frac{d^2 z}{dt^2} = -\frac{e}{m} [B_i(\mathbf{x}, t)v_x] \quad (14)$$

$$\mathbf{E}_{bias} = \frac{U_{bias}}{x \ln(b/a)} \mathbf{e}_x \quad (15)$$

where U_{bias} is the bias voltage between the inner conductor and outer conductor. Obviously, a positive voltage, $U_{bias} > 0$, corresponds to an electric field pointing from the inner conductor to the outer

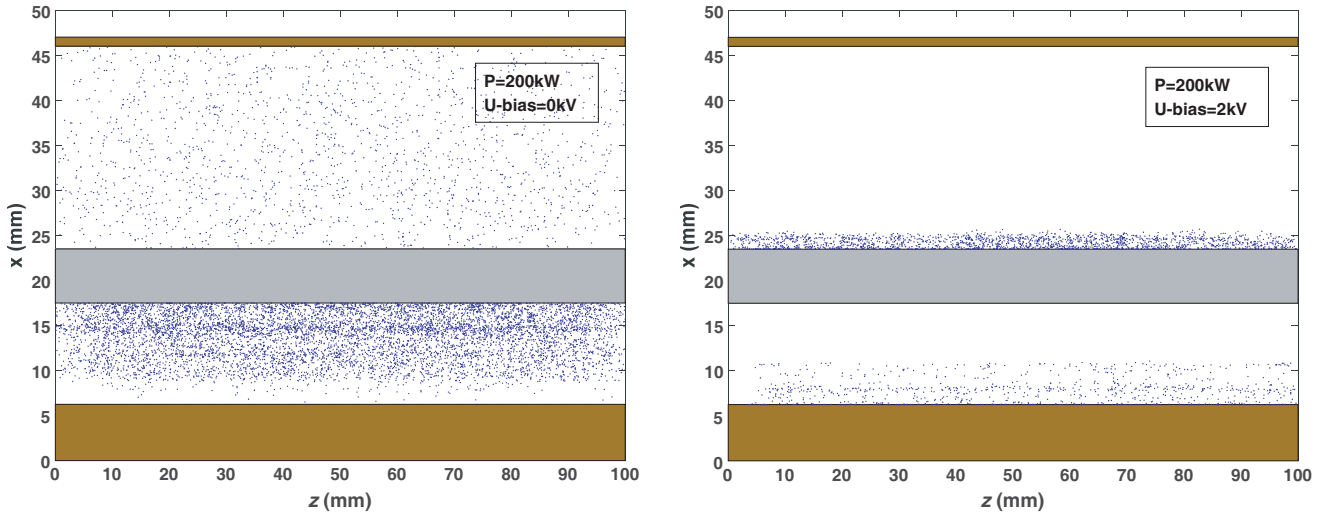


Figure 7. Evolution of the multipactor effect in coaxial line at different DC bias. $N_e = 6000$, transmission power $P = 200$ kW, frequency $f = 1.3$ GHz, transit time $t = 20$ T.

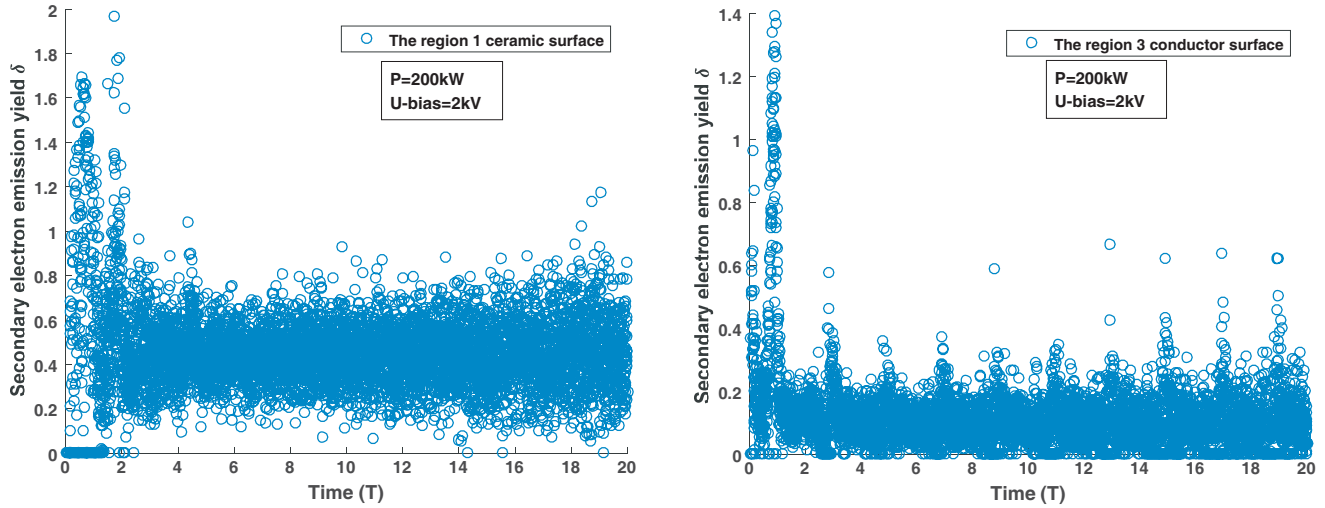


Figure 8. Evolution of SEE yield at different DC bias. $N_e = 6000$, transmission power $P = 200$ kW, frequency $f = 1.3$ GHz, transit time $t = 20$ T.

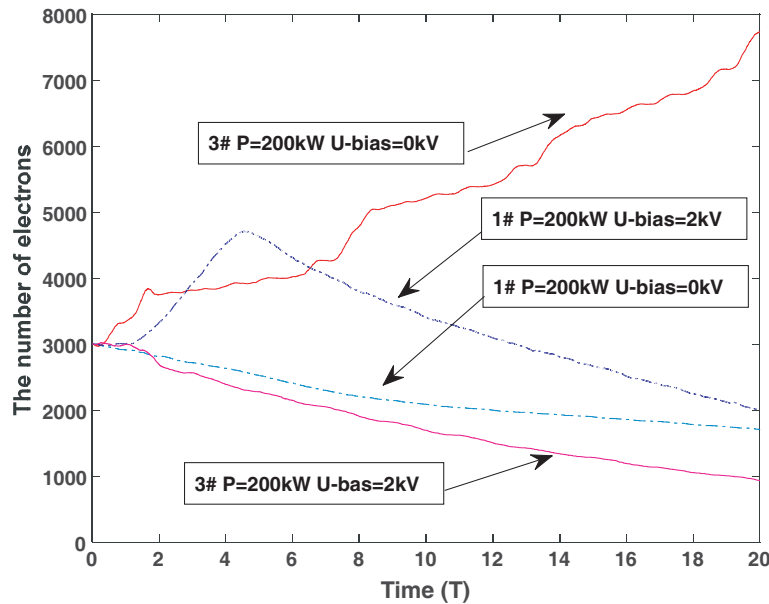


Figure 9. Evolution of the number of electrons at different DC bias. $N_e = 6000$, transmission power $P = 200$ kW, frequency $f = 1.3$ GHz, transit time $t = 20$ T.

conductor, and a negative voltage corresponds to an opposite field. The DC voltage can generate a repelling radial force, when being properly chosen, which breaks the resonant multipactor conditions. In the following, we analyze electron multipacting in coaxial line loaded ceramic window when the transmission power $P = 200$ kW at different U_{bias} .

In this part, the DC biasing voltage turns out to be an effective and simple method to suppress multipactor in coaxial lines. Fig. 7, Fig. 8, and Fig. 9 display the results of the analysis at the transmission power $P = 200$ kW after 20 periods. Fig. 7 shows the secondary electrons distribution of the multipactor after 20 periods at the same power and different bias voltages. Selecting a properly large bias voltage $U_{bias} = 2$ kV can generate a compensating trajectory and collision, which suppresses the secondary electron avalanche effectively. If the effect of an applied bias electric field results in the flight time of the electron is below two RF semi-periods, the resonance between the electron and the RF

electric field cannot be achieved, and consequently, no multipactor discharge is possible. Fig. 8 shows that the evolution of SEE yield at different U_{bias} when the transmission power $P = 200$ kW. Obviously, when the external U_{bias} is applied, the free electrons tend to move towards the inner conductor under the action of the electrostatic field. Thus, the collision electrons are mainly located on the surface of the ceramic and inner conductor, respectively. The secondary electron emission coefficients of the ceramic surface and inner conductor surface are about 0.5 and 0.16, respectively, shown in Figs. 8(a) and (b). Both of SEE yields are less than 1, which indicates that the multipactor growth is inhibited in this region, as shown in Fig. 9.

5. CONCLUSION

In this paper, firstly, we study the field pattern distribution of coaxial waveguide loaded ceramic and the motion mechanism of electrons in high-frequency fields under external U_{bias} . Secondly, the theory of secondary electron multiplication is introduced. Next, we discuss the development trend of secondary electron multiplication under different transmission powers, and the case under an application of an external DC bias field is studied theoretically and numerically by Monte Carlo (MC) simulation. Under high power transmission situation, the electrons get enough energy from the RF electric field, which will induce new secondary electrons on the surface of the structure. In region 3, due to the action of ponderomotive force, the electrons have the tendency to drift toward the outer conductor wall. Meanwhile, the application of an external U_{bias} with an appropriate amplitude is proposed to suppress the multipactor phenomenon in the RF field. Multipactor phenomenon can be understood in terms of the electron resonant trajectories. The resonance conditions can be destroyed by appropriate external electric field. If these secondary electrons cannot gain enough energy $W_i < W_1$ and are pulled back to the surface immediately, multipactor is subsequently suppressed during the collision. Thus, the application of an external DC bias to suppress the multipactor in coaxial line loaded ceramic is feasible.

ACKNOWLEDGMENT

We acknowledge the support of the National Natural Science Foundation of China (Grant No. 61531002) and National MCF Energy R&D Program (Grant No. 2018YFE0305100).

REFERENCES

1. Vaughan. J., "Multipactor," *IEEE Trans. Electron Devices*, Vol. 35, No. 7, 1172–1180, July 1988.
2. Semenov, V. E., E. I. Rakova, D. Anderson, M. Lisak, and J. Puech, *Phys. Plasmas*, Vol. 14, 033501, 2007.
3. Sazontov, A. G. and V. E. Nevchaev, *Phys. Plasmas*, Vol. 17, 033509, 2010.
4. Frotanpour, A., G. Dadashzadeh, M. Shahabadi, and B. Gimeno, *IEEE Trans. Electron Devices*, Vol. 58, 876, 2011.
5. Saito, Y., *IEEE Trans. Dielectr. Electr. Insul.*, Vol. 2, 243, 1995.
6. Padamsee, H., J. Knobloch, and T. Hays, *RF Superconductivity for Accelerators*, Wiley, Inc., New York, 1998.
7. Nayaiesh, A. R., E. L. Garwin, F. K. King, and R. E. Kirby, "Properties of thin anti-multipactor coatings for klystron windows," SLAC-PUB-3760, 1985.
8. Proch, D., D. Einfeld, R. Onken, and N. Steinhauser, "Measurement of multipacting currents of metal surfaces in RF fields," *IEEE Proceedings*, WPQ24, PAC 95, 1776, 1996.
9. YläOijala, P., "Suppressing electron multipacting in coaxial lines by DC voltage," *TESLA Reports 97-21*, 1–14, 1997.
10. YläOijala, P. and M. Ukkola, "Suppressing electron multipacting in ceramic windows by DC bias," *Nuclear Instruments & Methods in Physics Research, Section A, (Accelerators, Spectrometers, Detectors and Associated Equipment)*, Vol. 474, No. 3, 197–208, 2001.

11. Riyopoulos, S., "Multipactor saturation due to space-charge-induced debunching," *Physics of Plasmas*, Vol. 4, No. 5, 1448, 1997.
12. Li, Q., Y. H. Zhang, L. Qu, and Y. Fan, "Quasi-static analysis of multilayer dielectrics filled coaxial line using conformal mapping method," *2018 IEEE International Conference on Computational Electromagnetics (ICCEM)*, 2018.
13. Somersalo, E., P. Yla-Oijala, D. Proch, and J. Sarvas, "Computational methods for analyzing electron multipacting in RF structures," *Partiale Accel.*, Vol. 59, 107–141, August 1998.
14. Pérez, A. M., et al., "Prediction of multipactor breakdown thresholds in coaxial transmission lines for traveling, standing, and mixed waves," *IEEE Trans. Plasma Sci.*, Vol. 37, No. 10, 2031–2040, October 2009.
15. González-Iglesias, D., M. P. B. Rodríguez, Ò. M. Belda, and B. Gimeno, "Analysis of multipactor effect using a phase-shift keying single-carrier digital modulated signal," Vol. 60, No. 8, 2664–2670, August 2013.
16. Kishek, R. A. and Y. Y. Lau, *Phys. Rev. Lett.*, Vol. 80, 193, 1998.
17. Lau, Y. Y., R. A. Kishek, L. K. Ang, R. M. Gilgenbach, and A. Valfells, "Multipactor discharge on a dielectric," *IEEE International on Plasma Science, Anniversary*, IEEE, 2002.
18. Zhang, X., Y. Wang, and J. Fan, "The suppression effect of external magnetic field on the high-power microwave window multipactor phenomenon," *Physics of Plasmas*, Vol. 22, No. 2, 022110, 2015.
19. Saito, Y., "Surface breakdown phenomena in alumina RF windows," *IEEE Transactions on Dielectrics and Electrical Insulation*, Vol. 2, No. 2, 243–250, 1995.
20. Seviour, R., "The role of elastic and inelastic electron reflection in multipactor discharges," *IEEE Transactions on Electron Devices*, Vol. 52, No. 8, 1927–1930, 2005.
21. Chen, F. F., *Introduction to Plasma Physics*, Plenum Press, New York, 1974.
22. Gaponov, A. V. and M. A. Miller, "On the potential well for charged particles in a high-frequency electromagnetic field," *JETP Letters (translation of Pis'ma v Zhurnal Eksperimental'noi i Teoreticheskoi Fiziki)*, Vol. 7, 242–243, 1958.
23. Lobaev, M. A., O. A. Ivanov, V. A. Isaev, et al., "Effect of inhomogeneous microwave field on the threshold of multipactor discharge on a dielectric," *Technical Physics Letters*, Vol. 35, No. 12, 1074–1077, 2009.